Evidence for triaxial shape coexistence in ^{74}Ge

N. Sensharma,[1,2,*,†] A. D. Ayangeakaa,[1,2,‡] T. M. Kowalewski,[1,2] R. V. F. Janssens,[1,2] Y. M. Wang,[3] Q. B. Chen,[3] J. M. Allmond,[4] C. M. Campbell,[5] S. R. Carmichael,[6] M. P. Carpenter,[7] P. Copp,[7,§] C. Cousins,[8] M. Devlin,[9] U. Garg,[6] C. Müller-Gatermann,[7] D. J. Hartley,[10] J. Heery,[8] J. Henderson,[11,8] H. Jayatissa,[7,§] S. R. Johnson,[1,2] S. P. Kisyov,[11,‖] F. G. Kondev,[7] T. Lauritsen,[7] S. Nandi,[7] R. Rathod,[6] W. Reviol,[7] M. Rocchini,[12,¶] E. Rubino,[13] R. Russell,[8] A. Saracino,[1,2] D. Seweryniak,[7] M. Siciliano,[7] and C. Y. Wu[11]

[1]*Department of Physics and Astronomy, University of North Carolina Chapel Hill, North Carolina 27599, USA*
[2]*Triangle Universities Nuclear Laboratory, Duke University, Durham, North Carolina 27708, USA*
[3]*Department of Physics, East China Normal University, Shanghai 200241, China*
[4]*Physics Division, Oak Ridge National Laboratory, Oak Ridge, Tennessee 37831, USA*
[5]*Nuclear Science Division, Lawrence Berkeley National Laboratory, Berkeley, California 94720, USA*
[6]*Department of Physics and Astronomy, University of Notre Dame, Notre Dame, Indiana 46556, USA*
[7]*Physics Division, Argonne National Laboratory, Lemont, Illinois 60439, USA*
[8]*Department of Physics, University of Surrey, Surrey GU2 7XH, United Kingdom*
[9]*Physics Division, Los Alamos National Laboratory, Los Alamos, New Mexico 87545, USA*
[10]*Department of Physics, United States Naval Academy, Annapolis, Maryland 21402, USA*
[11]*Physics Division, Lawrence Livermore National Laboratory, Livermore, California 94550, USA*
[12]*Department of Physics, University of Guelph, Guelph, Ontario N1G 2W1, Canada*
[13]*Facility for Rare Isotope Beams, Michigan State University, East Lansing, Michigan 48824, USA*

(Received 31 October 2024; revised 2 April 2025; accepted 8 July 2025; published 4 August 2025)

The deformation properties of the low-lying states in ^{74}Ge have been investigated using multistep Coulomb excitation. The measurements were carried out with the advanced γ-ray tracking array, GRETINA, and the CHICO2 particle detector. A comprehensive set of $E2$ transition and diagonal matrix elements was deduced following an analysis with the semiclassical coupled-channels code GOSIA. The data were compared with results of calculations carried out within the framework of the generalized triaxial rotor model as well as with the configuration interaction shell model and the symmetric rotor model. Results from calculations with covariant density functional theory were used to construct a five-dimensional collective Hamiltonian for further comparisons with the data. Collectively, the calculations provide an accurate reproduction of the experimental matrix elements and further support an understanding in terms of the coexistence of two axially asymmetric shapes. This leads to an overall interpretation of the underlying structure of ^{74}Ge requiring triaxiality, as is also the case in the neighboring even-mass Ge isotopes.

DOI: 10.1103/h839-vb3z

I. INTRODUCTION

Shape coexistence is a notable phenomenon in nuclei within the $A \approx 60$–70 mass region, where the intrusion of the $g_{9/2}$ neutron orbital into the pf shell, combined with the effects of multiparticle excitations across the $Z = 28$ shell gap, leads to a variety of nuclear shapes and deformations at low energy. Several theoretical approaches [1–4] have predicted the coexistence of prolate and oblate shapes in these nuclei, occurring within a relatively constrained energy window of merely a few hundred kiloelectronvolts. These predictions have been further supported by the experimental observation of several low-lying excited 0^+ states in the even-even Ni, Zn, Ge, Se, and Kr isotopes. An interesting, albeit rarely observed, aspect of shape coexistence is the presence of multiple low-lying 0^+ states with triaxial characteristics. In the $A \approx 60$–70 region, the coexistence of two triaxial shapes associated with the $0^+_{1,2}$ states was established in ^{72}Ge following multistep Coulomb excitation measurements [5]. Progress in documenting the role of triaxiality and the complex interplay between single-particle and collective degrees of freedom contributing to the structural phenomena observed in these nuclei has come in no small part from recent advances in experimental techniques.

The even-even Ge isotopes have been the subject of extensive experimental and theoretical investigations due to the complexity of their low-spin structure. One of the earliest motivations for such studies stems from the work in Ref. [6]

*Present address: Physics Division, Argonne National Laboratory, Lemont, IL 60439, USA.
†Contact author: nsensharma@anl.gov
‡Contact author: ayangeak@unc.edu
§Present address: Los Alamos National Laboratory, Los Alamos, New Mexico 87545, USA.
‖Present address: Lawrence Berkeley National Laboratory, Berkeley, CA 94720, USA.
¶Present address: INFN Sezione di Firenze, Firenze I-50019, Italy.

 ©2025 American Physical Society

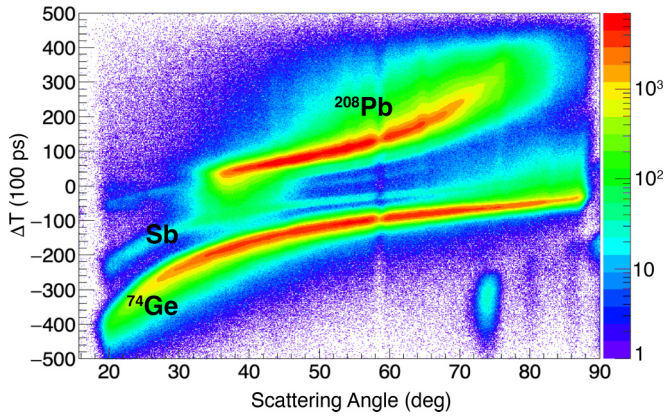

FIG. 1. Differences in time-of-flight (ΔT) between the projectile and target recoils as a function of the scattering angle θ measured with CHICO2. A clear separation between the ^{74}Ge and ^{208}Pb ions is observed. Contaminant Sb ions were also present in the beam but were removed in the analysis through coincidence gating (see text).

where the systematic behavior of the first excited 0^+ levels in even-even nuclei around $N, Z \approx 40$ was explained as resulting from the interplay between pairing and quadrupole correlations. Early on [7], it was also proposed that the presence of at least one excited 0^+ state in the low-energy structure of the stable even Ge isotopes, with properties different from the ground state, was an indication of shape coexistence due to the presence of intruder configurations.

Theoretically, a systematic investigation of the Ge isotopic chain spanning neutron numbers $N = 26$ to 76 was carried out in Ref. [8] within the Gogny-Hartree-Fock-Bogoliubov and Skyrme Hartree-Fock plus pairing in the Bardeen–Cooper–Schrieffer (BCS) approximation frameworks. Both models concurred on the prevalence of triaxial features across most Ge isotopes. Interestingly, the Skyrme HF plus BCS calculations identified possible shape-coexistent isomers in numerous Ge isotopes. However, these states were characterized by distinct shapes but minimal energy differences, perhaps more suggestive of γ softness than definite isomerism. Contrary to the anticipated γ softness in Ge nuclei, ^{76}Ge emerged as a rare exception, showcasing rigid triaxial deformation in its low-lying states [9–11]. Microscopic calculations employing the multiquasiparticle triaxial projected shell-model approach [12] supported this finding, affirming the necessity of a fixed triaxial deformation parameter, $\gamma \approx 30^\circ$, for an accurate description of ground-state and γ bands in this nucleus. Further analysis into the neighboring even isotopes ^{70,72,74,78,80}Ge underscored the enduring significance of triaxiality in elucidating the low-lying structure in these even-even Ge nuclei.

The ^{74}Ge nucleus has been investigated by Coulomb excitation in the earlier work of Toh *et al.* [13]. The five lowest-lying states were excited and the corresponding $E2$ matrix elements were determined. From the measured excitation energies and $B(E2)$ reduced transition probabilities, it was proposed that the 0_1^+, 2_1^+, and the 4_1^+ levels form a rotational band while the 0_2^+ state was associated with an intruder spherical band. However, in determining the quadrupole invariant $\langle Q^2 \rangle$ for this 0_2^+ state, Ref. [13] did not consider any level feeding into it. This resulted in a value consistent with zero and led to its classification as spherical. The 0_2^+ states of ^{72,76}Ge were also reported to be spherical in nature [7] until the work of Ref. [5], where a new $0_2^+ \rightarrow 2_3^+$ transition in ^{72}Ge was observed for the first time in a Coulomb excitation measurement, and the strong contribution from its matrix element resulted in a deformed 0_2^+ state with approximately the same $\langle Q^2 \rangle$ value as the ground state. For ^{76}Ge, however, the prediction of a spherical 0_2^+ holds based on the reported matrix elements and $B(E2)$ values in Refs. [10,11].

Contrary to the predictions of Ref. [6] and the results reported by earlier Coulomb excitation measurements for the even-even Ge isotopes, Ref. [5] showed that the shape transition between the first and the second 0^+ states occurs between ^{70}Ge and ^{72}Ge where the two states reverse character. However, such a transition is subtle with the two 0^+ levels acquiring similar deformation in ^{72}Ge. Following the work of Ref. [5], it became essential to reevaluate the low-lying structure of the next even-even Ge isotope, i.e., ^{74}Ge, and to investigate whether the original assertion of a spherical 0_2^+ state still holds for this isotope.

In this report, results on the low-lying structure and the quadrupole collectivity of ^{74}Ge, populated via multistep Coulomb excitation, are presented. Details of the measurement are given in Sec. II, while the data analysis and the experimental results are found in Sec. III. This is followed in Sec. IV by a discussion of the results and comparisons of

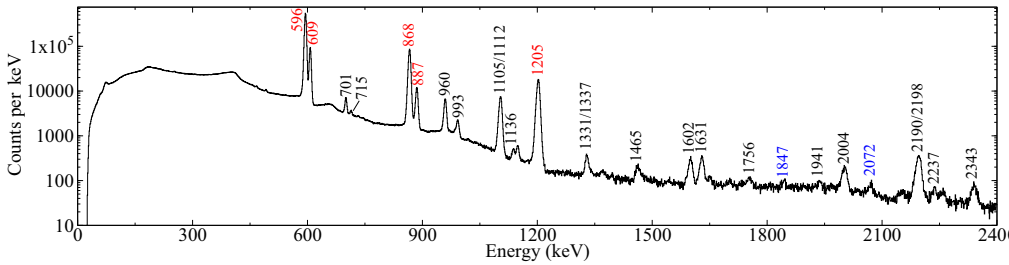

FIG. 2. Doppler-corrected γ-ray spectrum measured with GRETINA following Coulomb excitation of the ^{74}Ge beam on the ^{208}Pb target. Peaks marked in red were seen in a previous measurement [13] while those in black are observed for the first time in Coulomb excitation. The peaks marked in blue were not placed in the current level scheme and were also not used in the χ^2 minimization process (2072 $\sim$ sum peak 868 + 1205; 1847 $\sim$ sum peak 887 + 960).

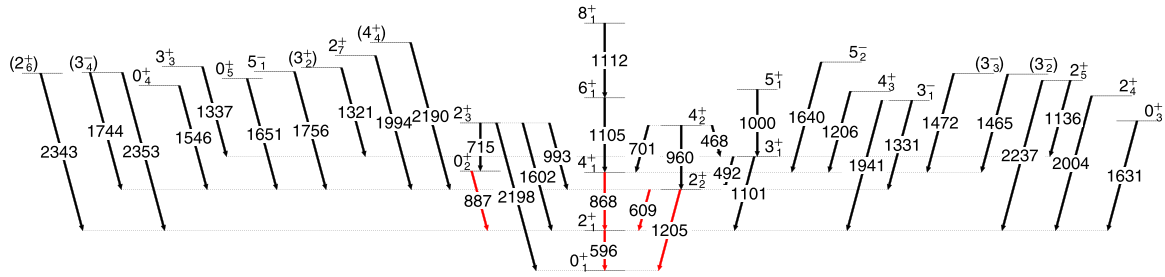

FIG. 3. Partial ^{74}Ge level scheme developed in the present Coulomb excitation measurement. Transitions marked in red were reported previously in Ref. [13]. All other γ rays were observed in a Coulomb excitation measurement for the first time in this work.

the experimental data with the generalized triaxial rotor model (GTRM) and large-scale shell-model calculations, as well as covariant density functional theory.

II. EXPERIMENT

Low-lying states of ^{74}Ge were populated via multistep Coulomb excitation in an experiment performed at the ATLAS accelerator facility at Argonne National Laboratory. A 300-MeV ^{74}Ge beam bombarded a 0.44-mg/cm^2 ^{208}Pb target. The γ rays emitted in the deexcitation process were detected by the GRETINA tracking array [14], in kinematic coincidence with scattered reaction products registered with CHICO2, a two-dimensional, pixelated parallel-plate avalanche counter [15]. With a total solid-angle coverage of $\approx 69\%$, CHICO2 covers laboratory scattering angles between 20°–85° in the forward and 96°–164° in the backward directions with an angular resolution of 1.55° in θ and 2.47° in ϕ. CHICO2 also maintains a mass resolution ($\Delta m/m$) of $\approx 5\%$ which facilitates the separation of scattered weak beams from scattered contaminant ones. A time resolution (FWHM) of $\approx$1.2 ns achieved with this detector enables the measurement of the time-of-flight differences (ΔT) between the scattered reaction products as a function of the polar scattering angle θ. A two-dimensional histogram of ΔT as a function of θ illustrating the clear separation between the reaction products is displayed in Fig. 1. Due to some leftover antimony (Sb) in the beam during the experiment, Sb ions were also scattered and are seen as a contaminant in this figure. These were removed in the analysis through coincidence gating. At the time of this measurement, the GRETINA array consisted of 47 highly segmented, high-purity germanium (HPGe) detectors, grouped into 12 modules. The chosen beam energy of 300 MeV is slightly higher than the so-called safe energy of $\approx$290 MeV. While the safe-energy criterion ensures a purely electromagnetic interaction by maintaining a minimum separation of 5 fm between the nuclear surfaces, the choice of slightly higher beam energy was made to enhance the population of high-spin states in the ground-state and γ bands.[1]

Event-by-event reconstruction of the reaction kinematics and accurate Doppler correction of the in-flight γ-ray energies was made possible by the time and angular resolution offered by CHICO2 and the position information obtained from GRETINA. Figure 2 provides a sample Doppler-reconstructed spectrum acquired in coincidence with the scattered ^{74}Ge recoils. In total, 37 γ rays connecting 28 low-lying states in ^{74}Ge were measured. A partial level scheme incorporating most of these transitions is given in Fig. 3. The five transitions highlighted in red are those observed in a previous Coulomb excitation measurement [13]. The transitions marked in black are observed in Coulomb excitation for the first time. Spin and parity quantum numbers for all levels displayed in Fig. 3 were adopted from earlier studies where the ^{74}Ge energy levels were investigated via scattering [16–18], decay [19], transfer [20,21], and neutron capture [22].

III. DATA ANALYSIS AND RESULTS

The measured γ-ray yields were analyzed using the semiclassical, coupled-channels Coulomb excitation least-squares search code, GOSIA [23,24]. The level scheme of Fig. 3 presents a number of γ-ray transitions that were too close in energy and could not be resolved (the 1205- and 1206-keV and the 1331- and 1337-keV γ rays). These transitions were treated by specifying their combined yield in the input data; i.e., instead of fitting individual transitions separately, the total observed yield was assigned to the unresolved doublet, and the GOSIA code used this combined value along with the spectroscopic branching ratio to optimize the fit, hence, considering the contributions from both transitions. Given a starting set of transition and diagonal matrix elements, GOSIA then constructs a standard χ^2 function by comparing the measured γ-ray yields to those predicted theoretically. The Coulomb-excitation cross sections depend on the relative phases, the signs, and the magnitude of the matrix elements. A random set of matrix elements was used to initiate the χ^2-minimization process. Moreover, matrix elements corresponding to all in-band transitions of the ground state and the γ bands were assigned a positive sign. The signs of all other matrix elements were determined relative to these and varied during the χ^2-fitting process to avoid possible trapping in local χ^2 minima. As mentioned in Ref. [5], the absolute signs of transition matrix elements are not experimental observables. However, the signs of the diagonal matrix elements determine whether the deformation is prolate or oblate.

[1]At $E_{\text{beam}} = 300$ MeV, the separation between the nuclei corresponds to 4.4 fm. This 0.6 fm reduction in the safe distance is insufficient to make the contributions of nuclear force significant. The observed cross sections, thus, result from a purely electromagnetic interaction.

To increase the sensitivity of the measurements, the data were partitioned into six angular subsets, corresponding to laboratory scattering angular ranges of 30°–45°, 45°–60°, 60°–75°, 75°–85°, 95°–131°, and 131°–168°. This resulted in a total of 138 efficiency-corrected γ-ray intensities associated with the different scattering angles. In Fig. 4, spectra demonstrating the angular dependence are displayed for forward (30°–45°, 45°–60°, 60°–75°, and 75°–85°) and backward (95°–131° and 131°–168°) angular ranges. This figure illustrates the sensitivity to transitions between the higher-spin states achieved as the particle scattering angle increases from 30° to 168°.

Finally, available spectroscopic data such as lifetimes (τ), branching ratios, and $E2/M1$ mixing ratios (δ) were included as constraints of the key parameters during the fitting procedure. The lifetimes and mixing ratios used in the present analysis are provided in Table I while the branching ratios are listed in Table II. The spectroscopic data, as reproduced by GOSIA, are provided in the third column of both tables.

A total of 111 $E1, E2, E3$, and $M1$ reduced matrix elements was determined. Figure 5 compares the measured γ-ray yields with those calculated from GOSIA for the four most intense transitions, viz., the $2_1^+ \rightarrow 0_1^+$, $2_2^+ \rightarrow 2_1^+$, $4_1^+ \rightarrow 2_1^+$, and $0_2^+ \rightarrow 2_1^+$ ones. The final set of matrix elements, which most accurately reproduces the experimental γ-ray yields and the available spectroscopic data, can be found in Table III. The quoted uncertainties for matrix elements were derived by constructing a probability distribution in the space of fitted parameters and requesting the total probability to be equal to the chosen 1σ confidence limit (68.3%). These uncertainties include statistical, systematic, and cross-correlation contributions. The systematic errors, which arise from factors such as stopping power, γ-ray efficiency, and detector geometry offsets, contribute a global error of 4–5%, added in quadrature to the statistical uncertainties.

IV. DISCUSSION

A. Matrix elements and transitions strengths

The transition matrix elements obtained from the present study are in satisfactory agreement with results from previous Coulomb excitation measurements such as those of Refs. [13] and [26] (see columns 3, 4, and 5 of Table III). The only notable exceptions relate to the matrix elements associated with the 0_2^+ state. For the $0_2^+ \rightarrow 2_1^+$ and $0_2^+ \rightarrow 2_2^+$ transitions, Ref. [13] reported matrix elements with magnitudes of $+0.14(4)$ eb and $0.00(11)$ eb, respectively. In the present study, these matrix elements were observed with significantly larger magnitudes: $0.228^{+0.005}_{-0.004}$ eb and $-0.18(2)$ eb, respectively. The discrepancy is likely due to a contribution from the newly observed 2_3^+ level which decays via the 715-keV transition to the 0_2^+ level. This 2198-keV, 2_3^+ state and its connection to the 0_2^+ level are observed here for the first time. The spectroscopic quadrupole moments obtained from the diagonal matrix elements of the 2_1^+ and 2_2^+ levels also agree well with those of Refs. [13,26]. The reduced transition probabilities deduced from the matrix elements are provided

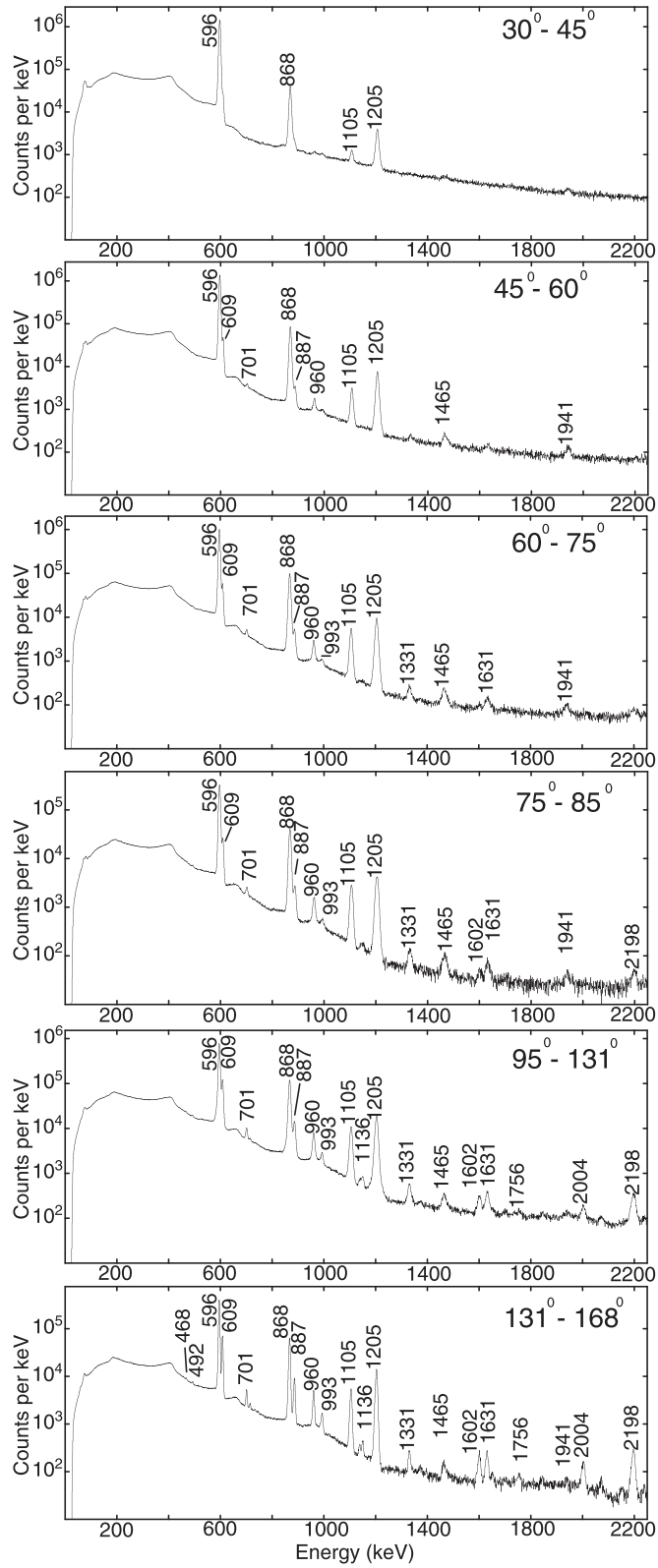

FIG. 4. Spectra obtained from Coulomb excitation of ^{74}Ge on ^{208}Pb for the subsets of data corresponding to forward (30°–45°, 45°–60°, 60°–75°, and 75°–85°) and backward (95°–131° and 131°–168°) ranges of particle-scattering angles θ.

TABLE I. Lifetimes (τ) and mixing ratios (δ) used to constrain the χ^2 minimization process in GOSIA. Data were taken from ENSDF [24]. The values, as reproduced by GOSIA after the χ^2-minimization process, are presented as well.

I^π	Lifetime (τ) (ps)	GOSIA value
2_1^+	17.90 ± 0.13	17.92
4_1^+	2.21 ± 0.14	1.91
6_1^+	0.75 ± 0.81	0.69
0_2^+	3.7 ± 2.2	2.86
2_2^+	7.80 ± 1.15	6.54
2_3^+	1.61 ± 0.27	1.59
2_7^+	0.035 ± 0.012	0.034
$I_i^\pi \to I_f^\pi$	Mixing ratio (δ)	GOSIA value
$2_2^+ \to 2_1^+$	2.98 ± 0.27	2.97
$4_2^+ \to 4_1^+$	0.84 ± 0.11	0.85
$3_1^+ \to 2_1^+$	5.84 ± 0.60	5.80
$4_2^+ \to 3_1^+$	1.06 ± 0.91	0.71
$3_1^+ \to 2_2^+$	2.07 ± 0.15	2.06

in the last two columns of Table III. The present $B(E2)$ values are in good agreement with those determined from $(n, n'\gamma)$ measurements by Ref. [25] (given in the last column of Table III). The extracted diagonal matrix elements for the 2_1^+, 4_1^+, and 6_1^+ levels in the ground-state band are negative. This is consistent with a prolate deformation for the ground-state band. Likewise, the positive sign and the magnitude deduced for the diagonal matrix element of the 2_2^+ state in the γ band are both in line with a prolate deformation as well. This matrix element is also in agreement with the value reported in Ref. [13]. The data obtained in the present work were, however, not found to be sensitive to the matrix elements associated with the 5_1^+ level in the γ band as well as to the diagonal matrix element of the 8_1^+ level in the ground-state band. Hence, there are no corresponding matrix elements in Table III.

TABLE II. Branching ratios (BR) used to constrain the χ^2-minimization process in GOSIA. Data were taken from ENSDF [24]. The values predicted by GOSIA following the χ^2-minimization process are given as well.

$\frac{I_i^\pi \to I_{f1}^\pi}{I_i^\pi \to I_{f2}^\pi}$	BR $[\frac{I(I_i^\pi \to I_{f1}^\pi)}{I(I_i^\pi \to I_{f2}^\pi)}]$	GOSIA value
$\frac{2_2^+ \to 0_1^+}{2_2^+ \to 2_1^+}$	0.46 (3)	0.45
$\frac{3_1^+ \to 2_2^+}{3_1^+ \to 2_1^+}$	0.58 (1)	0.47
$\frac{4_2^+ \to 3_1^+}{4_2^+ \to 2_2^+}$	0.065 (3)	0.07
$\frac{4_2^+ \to 4_1^+}{4_2^+ \to 2_2^+}$	0.43 (1)	0.48
$\frac{2_3^+ \to 0_2^+}{2_3^+ \to 2_2^+}$	0.35 (3)	0.36
$\frac{3_4^- \to 2_2^+}{3_4^- \to 2_1^+}$	0.108 (4)	0.108

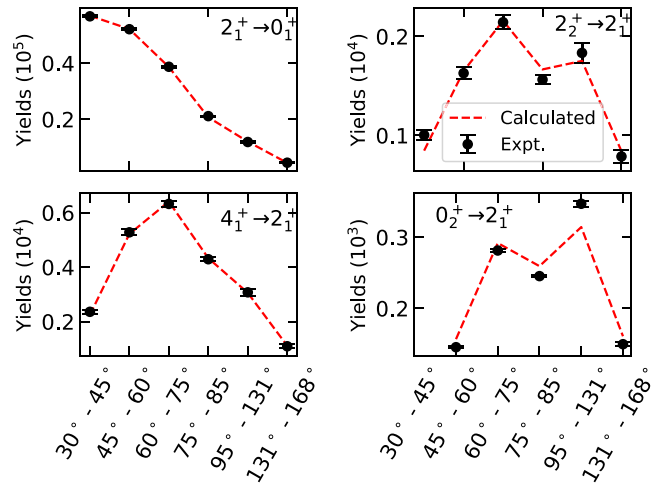

FIG. 5. Calculated and experimental yields for the $2_1^+ \to 0_1^+$, $2_2^+ \to 2_1^+$, $4_1^+ \to 2_1^+$, and $0_2^+ \to 2_1^+$ transitions as obtained after the χ^2 minimization process.

The relatively large values determined for the intraband matrix elements associated with the ground-state and γ bands are indicative of a moderately collective structure for both bands. This is confirmed further by the corresponding reduced $B(E2)$ transition probabilities with values up to $\approx$ 100 W.u. Finally, the $\langle 2_1^+ || \mathcal{M}(E2) || 2_2^+ \rangle$ matrix element was also deduced to have a large magnitude ($\approx$0.68 eb). As discussed below, this indicates broken axial symmetry and enables strong mixing between the underlying $I = 2$ states in the ground-state and γ bands.

B. Triaxial rotor model calculations

In order to gain further insight into the newly deduced $E2$ matrix elements and the structure of the low-lying states in ^{74}Ge, the GTRM with independent inertia and electric quadrupole tensors was employed first [27–31]. Using GTRM, the $E2$ matrix elements for levels within the ground-state and the γ bands were calculated with a minimum set of assumptions and compared to the experimental results. The three model parameters required to describe these $E2$ matrix elements of the triaxial rotor include the intrinsic quadrupole deformation, Q_0, the asymmetry or triaxiality of the electric quadrupole tensor, γ, and the asymmetry or mixing angle of the inertia tensor, Γ. These parameters were determined analytically from the experimental matrix elements: $\langle 0_1 || \mathcal{M}(E2) || 2_1 \rangle$, $\langle 0_1 || \mathcal{M}(E2) || 2_2 \rangle$, and $\langle 2_1 || \mathcal{M}(E2) || 2_1 \rangle$, yielding $Q_0 = 1.77(1)\,e$b, $\gamma = 28(1)^\circ$, and $\Gamma = -19(1)^\circ$, respectively.

Figures 6(a)–6(d) compare the experimental results for the transition and diagonal matrix elements of the ground-state and γ bands with those obtained from the GTRM. It is important to note that the large value of the mixing parameter, $\Gamma = -19^\circ$, suggests significant mixing, which renders the two-band approximation of the GTRM (as described in Ref. [32]) inadequate at medium to high spins. To address this issue, a full diagonalization of the triaxial rotor was implemented to accurately reproduce the experimental

TABLE III. Summary of $E1$, $E2$, $E3$, and $M1$ matrix elements and reduced transition probabilities for ^{74}Ge deduced in the present work. Units for reduced transition strengths are μ_N^2, $e^2\,\mathrm{b}$, $e^2\,\mathrm{b}^2$, and $e^2\,\mathrm{b}^3$ for the $M1$, $E1$, $E2$, and $E3$ transitions, respectively. Accordingly, the $E1$, $E2$, $E3$, and $M1$ matrix elements are listed in units of $e\,\mathrm{b}^{1/2}$, $e\,\mathrm{b}$, $e\,\mathrm{b}^{3/2}$, and μ_N. Here λ denotes either E or M and L takes values of 1, 2, or 3. The last two columns present the reduced transition probabilities in Weisskopf units (W.u.) derived in the present work and those reported in Ref. [25].

	E_γ (keV)		$\langle I_i \| \mathcal{M}(\lambda L) \| I_f \rangle$				$B(\lambda L; I_f^\pi \to I_i^\pi)$ [W.u.]	
$I_i^\pi \to I_f^\pi$	(observed)	Mult.	This work	Ref. [13]	Ref. [26]	$B(\lambda L; I_f^\pi \to I_i^\pi)$	This work	Ref. [25]
$0_1^+ \to 2_1^+$	596	$E2$	$0.550^{+0.003}_{-0.002}$	0.551(2)	0.5500(27)	0.061(1)	32.8(3)	
$0_1^+ \to 2_2^+$	1205	$E2$	$0.087^{+0.001}_{-0.002}$	0.058(10)	|0.081(14)|	0.0015(1)	0.83(3)	
$0_1^+ \to 2_3^+$	2198	$E2$	$0.041^{+0.003}_{-0.004}$			0.0003(1)	0.18(3)	0.168(27)
$0_1^+ \to 3_1^-$		$E3$	−0.10(4)			0.002(1)	5(4)	
$0_1^+ \to 3_2^-$		$E3$	0.12(4)			0.002(1)	6(4)	
$0_1^+ \to 3_3^-$		$E3$	$0.21^{+0.07}_{-0.44}$			$0.006^{+0.005}_{-0.006}$	19^{+14}_{-19}	
$0_1^+ \to 3_4^-$		$E3$	−0.21(6)			0.006(4)	20(14)	
$2_1^+ \to 2_1^+$		$E2$	$-0.28^{+0.02}_{-0.03}$	−0.25(3)[a]	−0.36(9)[b]			
$2_1^+ \to 4_1^+$	868	$E2$	0.884(7)	0.850(25)	|0.77(4)|	0.087(1)	47.0(7)	38(11)
$2_1^+ \to 2_2^+$	609	$E2$	$0.682^{+0.009}_{-0.006}$	0.50(4)	|0.71(7)|	0.093(2)	$50.3^{+1.3}_{-0.8}$	
$2_1^+ \to 2_2^+$	609	$M1$	0.11(1)			$0.0027^{+0.0006}_{-0.0003}$	$0.0015^{+0.0003}_{-0.0002}$	
$2_1^+ \to 3_1^+$	1101	$E2$	$0.102^{+0.011}_{-0.003}$			0.0015(1)	$0.81^{+0.18}_{-0.05}$	<3.0
$2_1^+ \to 3_1^+$	1101	$M1$	$0.016^{+0.003}_{-0.002}$			0.00004(1)	0.00002(1)	<0.00014 μ_N^2
$2_1^+ \to 0_2^+$	887	$E2$	$0.228^{+0.005}_{-0.004}$	0.14(4)	$\lvert < 0.2 \rvert$	0.052(2)	28(1)	21.9(83)
$2_1^+ \to 2_3^+$	1602	$E2$	$0.03^{+0.01}_{-0.03}$			0.0001(2)	$0.08^{+0.09}_{-0.08}$	0.320^{+55}_{-54}
								0.0129^{+55}_{-46}
$2_1^+ \to 2_3^+$	1602	$M1$	0.09(1)			0.0015(5)	0.0008(3)	0.000044^{+25}_{-17} μ_N^2
								0.00106^{+18}_{-17} μ_N^2
$2_1^+ \to 2_4^+$	2004	$E2$	$-0.07^{+0.01}_{-0.03}$			0.001(1)	0.5(5)	0.000006^{+460}_{-6}
$2_1^+ \to 2_4^+$	2004	$M1$	0.4(1.0)			<0.20	<0.1	0.0083^{+10}_{-9} μ_N^2
$2_1^+ \to 2_5^+$	2237	$E2$	$-0.14^{+0.04}_{-0.03}$			0.004(2)	2.0(9)	0.005^{+58}_{-5}
								23.0^{+17}_{-16}
$2_1^+ \to 2_5^+$	2237	$M1$	$-0.4^{+1.0}_{-0.4}$			$0.03^{+0.10}_{-0.03}$	$0.02^{+0.06}_{-0.02}$	0.176(8) μ_N^2
								0.0277^{+56}_{-49} μ_N^2
$2_1^+ \to 2_6^+$	2343	$E2$	$-0.12^{+0.07}_{-0.04}$			0.003(2)	2(1)	
$2_1^+ \to 2_6^+$	2343	$M1$	<0.5			<0.2	<0.1	
$2_1^+ \to 2_7^+$		$E2$	$0.27^{+0.16}_{-0.06}$			$0.01^{+0.02}_{-0.01}$	8^{+12}_{-3}	0.029^{+28}_{-17}
$2_1^+ \to 2_7^+$		$M1$	0.1(4)			<0.03	<0.02	0.00210^{+34}_{-36} μ_N^2
$2_1^+ \to 0_3^+$	1631	$E2$	−0.05(1)			0.003(1)	1.4(7)	<0.62
$2_1^+ \to 4_3^+$		$E2$	−0.01(5)			<0.0004	<0.19	0.81^{+22}_{-21}
$2_1^+ \to 4_4^+$		$E2$	−0.09(5)			0.001(1)	$0.5^{+0.6}_{-0.5}$	
$2_1^+ \to 0_4^+$		$E2$	0.27(7)			$0.07^{+0.04}_{-0.03}$	40^{+24}_{-18}	0.55^{+18}_{-17}
$2_1^+ \to 0_5^+$		$E2$	<0.15			<0.03	<21	1.16^{+12}_{-11}
$2_1^+ \to 3_1^-$	1941	$E1$	$-0.030^{+0.004}_{-0.014}$			$0.0001^{+0.0002}_{-0.0001}$	0.01(1)	0.173^{+17}_{-16} mW.u.
$2_1^+ \to 3_4^-$	2353	$E1$	$0.180^{+0.018}_{-0.004}$			$0.0047^{+0.0010}_{-0.0002}$	$0.41^{+0.08}_{-0.02}$	0.0444^{+77}_{-73} mW.u.
$4_1^+ \to 4_1^+$		$E2$	$-0.24^{+0.03}_{-0.04}$					
$4_1^+ \to 6_1^+$	1105	$E2$	$0.96^{+0.03}_{-0.02}$			$0.071^{+0.004}_{-0.003}$	39(2)	36^{+20}_{-18}
$4_1^+ \to 2_2^+$		$E2$	$0.30^{+0.02}_{-0.01}$	0.05(25)		$0.018^{+0.003}_{-0.001}$	10(1)	
$4_1^+ \to 4_2^+$	701	$E2$	$0.54^{+0.03}_{-0.04}$			$0.032^{+0.003}_{-0.004}$	18(2)	22^{+14}_{-11}
								1.0^{+21}_{-8}
$4_1^+ \to 4_2^+$	701	$M1$	$0.37^{+0.03}_{-0.02}$			$0.015^{+0.003}_{-0.002}$	$0.009^{+0.002}_{-0.001}$	0.020^{+12}_{-9} μ_N^2
								0.033^{+15}_{-14} μ_N^2
$4_1^+ \to 3_1^+$		$E2$	$0.02^{+0.09}_{-0.10}$			<0.002	<0.9	<66
$4_1^+ \to 3_1^+$		$M1$	$0.1^{+0.2}_{-0.4}$			<0.01	<0.01	<0.0053 μ_N^2

TABLE III. (*Continued.*)

$I_i^\pi \to I_f^\pi$	E_γ (keV) (observed)	Mult.	$\langle I_i\|\|\mathcal{M}(\lambda L)\|\|I_f\rangle$ This work	Ref. [13]	Ref. [26]	$B(\lambda L; I_f^\pi \to I_i^\pi)$	$B(\lambda L; I_f^\pi \to I_i^\pi)$ [W.u.] This work	Ref. [25]
$4_1^+ \to 2_3^+$		$E2$	0.14(5)			$0.004^{+0.003}_{-0.002}$	2^{+2}_{-1}	5.15^{+88}_{-85}
$4_1^+ \to 4_3^+$	1206	$E2$	$0.84^{+0.11}_{-0.09}$			0.08(2)	43^{+12}_{-9}	
$4_1^+ \to 4_3^+$	1206	$M1$	$-0.2^{+0.8}_{-0.7}$			$0.003^{+0.070}_{-0.003}$	$0.001^{+0.041}_{-0.001}$	
$4_1^+ \to 5_1^-$		$E1$	$0.06^{+0.02}_{-0.04}$			$0.0003^{+0.0002}_{-0.0003}$	$0.03^{+0.02}_{-0.03}$	
$4_1^+ \to 3_3^-$	1472	$E1$	$0.0003^{+0.0001}_{-0.0006}$			$\sim 10^{-8}$	$\sim 10^{-6}$	0.086^{+54}_{-52} mW.u.
$4_1^+ \to 3_2^-$	1465	$E1$	$0.10^{+0.01}_{-0.02}$			$0.0015^{+0.0003}_{-0.0004}$	$0.13^{+0.03}_{-0.04}$	
$6_1^+ \to 6_1^+$		$E2$	$\geqslant -0.12$					
$6_1^+ \to 8_1^+$	1112	$E2$	$1.8^{+0.1}_{-0.2}$			$0.20^{+0.03}_{-0.04}$	107^{+15}_{-21}	
$6_1^+ \to 4_2^+$		$E2$	$0.62^{+0.07}_{-0.05}$			0.04(1)	23^{+6}_{-4}	
$2_2^+ \to 2_2^+$		$E2$	0.27(2)	0.35(8)[a]				
$2_2^+ \to 4_2^+$	960	$E2$	0.55(2)			$0.033^{+0.003}_{-0.002}$	18^{+2}_{-1}	22.4(94)
$2_2^+ \to 3_1^+$	492	$E2$	$0.48^{+0.06}_{-0.02}$			$0.032^{+0.007}_{-0.002}$	18^{+4}_{-1}	<130
$2_2^+ \to 3_1^+$	492	$M1$	$0.095^{+0.003}_{-0.004}$			0.0013(1)	0.0007(1)	$<0.0096\ \mu_N^2$
$2_2^+ \to 0_2^+$		$E2$	−0.18(2)	0.00(11)		0.034(8)	18(4)	
$2_2^+ \to 2_3^+$	993	$E2$	$0.13^{+0.02}_{-0.03}$			0.004(1)	1.9(7)	1.64^{+95}_{-59}
								5.4(15)
$2_2^+ \to 2_3^+$	993	$M1$	0.22(1)			0.010(1)	0.005(1)	$0.0117^{+24}_{-25}\ \mu_N^2$
								$0.0070^{+23}_{-17}\ \mu_N^2$
$2_2^+ \to 0_3^+$		$E2$	$-0.09^{+0.06}_{-0.09}$			$0.01^{+0.02}_{-0.01}$	5^{+12}_{-5}	<5.7
$2_2^+ \to 4_3^+$		$E2$	0.03(6)			<0.001	<0.39	
$2_2^+ \to 4_4^+$	2190	$E2$	$0.50^{+0.19}_{-0.14}$			$0.03^{+0.02}_{-0.01}$	15^{+13}_{-7}	
$2_2^+ \to 2_4^+$		$E2$	$0.2^{+0.1}_{-0.3}$			$0.006^{+0.005}_{-0.006}$	3(3)	0.243^{+49}_{-52}
								0.084^{+54}_{-34}
$2_2^+ \to 2_4^+$		$M1$	−0.0(7)			<0.1	<0.1	$0.000029^{+64}_{-22}\ \mu_N^2$
								$0.00043(14)\ \mu_N^2$
$2_2^+ \to 2_5^+$		$E2$	<0.4			<0.03	<14	⩽4.3
$2_2^+ \to 2_5^+$		$M1$	<0.4			<0.1	<0.1	$\leqslant 0.015\ \mu_N^2$
$2_2^+ \to 2_6^+$		$E2$	<0.19			<0.01	<7	
$2_2^+ \to 2_6^+$		$M1$	−0.0(7)			<0.1	<0.1	
$2_2^+ \to 2_7^+$	1994	$E2$	$-0.2^{+0.1}_{-0.2}$			$0.01^{+0.03}_{-0.01}$	6^{+15}_{-6}	0.0003^{+120}_{-3}
								2.39^{+27}_{-25}
$2_2^+ \to 2_7^+$	1994	$M1$	<0.4			<0.1	<0.1	$0.0144(10)\ \mu_N^2$
								$0.00210^{+68}_{-57}\ \mu_N^2$
$2_2^+ \to 0_5^+$	1651	$E2$	$-0.13^{+0.19}_{-0.05}$			0.02(1)	9(8)	6.74^{+64}_{-59}
$2_2^+ \to 0_4^+$	1546	$E2$	$-0.11^{+0.11}_{-0.05}$			0.01(1)	6^{+8}_{-6}	1.43^{+49}_{-45}
$2_2^+ \to 3_1^-$	1331	$E1$	$0.20^{+0.04}_{-0.03}$			$0.005^{+0.003}_{-0.002}$	$0.48^{+0.22}_{-0.14}$	0.140^{+16}_{-15} mW.u.
$2_2^+ \to 3_4^-$	1744	$E1$	$0.093^{+0.003}_{-0.001}$			$0.00124^{+0.00006}_{-0.00004}$	$0.109^{+0.006}_{-0.004}$	0.0099^{+21}_{-19} mW.u.
$2_2^+ \to 5_2^-$		$E3$	<0.3			<0.01	<24	
$4_2^+ \to 4_2^+$		$E2$	$-0.45^{+0.08}_{-0.10}$					
$4_2^+ \to 3_1^+$	468	$E2$	$0.51^{+0.13}_{-0.09}$			$0.04^{+0.02}_{-0.01}$	20^{+12}_{-6}	17^{+22}_{-12}
$4_2^+ \to 3_1^+$	468	$M1$	0.28(4)			0.011(3)	0.006(2)	$0.0043^{+56}_{-33}\ \mu_N^2$
$3_1^+ \to 3_1^+$		$E2$	0.0(7)					
$3_1^+ \to 3_2^+$	1321	$E2$	<0.8			<0.14	<77	0.05^{+60}_{-5}
$3_1^+ \to 3_2^+$	1321	$M1$	$0.1^{+0.9}_{-1.2}$			<0.2	<0.1	$0.0172^{+16}_{-25}\ \mu_N^2$
$3_1^+ \to 3_3^+$	1337	$E2$	<0.6			<0.13	<69	$0.00067 - 0.0012$
								$0.97 - 1.8$
$3_1^+ \to 3_3^+$	1337	$M1$	0.0(1.0)			<0.15	<0.1	$0.0032 - 0.0058\ \mu_N^2$
								$0.00096 - 0.0018\ \mu_N^2$

TABLE III. (*Continued.*)

$I_i^\pi \to I_f^\pi$	E_γ (keV) (observed)	Mult.	$\langle I_i\|\|\mathcal{M}(\lambda L)\|\|I_f\rangle$ This work	Ref. [13]	Ref. [26]	$B(\lambda L; I_f^\pi \to I_i^\pi)$	$B(\lambda L; I_f^\pi \to I_i^\pi)$ [W.u.] This work	Ref. [25]
$3_1^+ \to 2_5^+$	1136	$E2$	$0.1^{+0.5}_{-0.6}$			<0.1	<37	
$3_1^+ \to 2_5^+$	1136	$M1$	0.0(4)			<0.03	<0.02	
$0_2^+ \to 2_3^+$	715	$E2$	$0.41^{+0.03}_{-0.01}$			$0.033^{+0.005}_{-0.002}$	18^{+3}_{-1}	19.8^{+32}_{-31}
$0_2^+ \to 2_7^+$		$E2$	$-0.01^{+0.09}_{-0.10}$			<0.003	<1.4	
$0_2^+ \to 2_4^+$		$E2$	0.05(9)			$0.0005^{+0.0030}_{-0.0005}$	$0.3^{+1.8}_{-0.3}$	
$0_2^+ \to 2_5^+$		$E2$	$0.07^{+0.20}_{-0.10}$			$0.001^{+0.013}_{-0.001}$	<7	
$0_2^+ \to 2_6^+$		$E2$	$-0.20^{+0.14}_{-0.16}$			$0.01^{+0.02}_{-0.01}$	4^{+10}_{-4}	
$2_3^+ \to 2_3^+$		$E2$	$0.02^{+0.18}_{-0.10}$					
$2_3^+ \to 0_3^+$		$E2$	$0.06^{+0.09}_{-0.06}$			$0.004^{+0.020}_{-0.004}$	2^{+10}_{-2}	

[a]Calculated from the spectroscopic quadrupole moment of Ref. [13].
[b]Calculated from the spectroscopic quadrupole moment of Ref. [26].

transition matrix elements. For completeness, calculations using the symmetric rotor model are also included for comparison. The transition matrix elements for the ground-state and the γ bands are reasonably reproduced by both the symmetric rotor model and the GTRM, as depicted in Figs. 6(a) and 6(b). This consistency arises from the fact that both versions of the rotor model inherently permit intraband transitions within the bands. However, at higher-spin states (4_1^+ and above), notable deviations start appearing between the experimental values and the calculations. On the other hand, Figs. 6(c) and 6(d) demonstrate that only the GTRM satisfactorily reproduces the diagonal matrix elements. This agreement highlights the necessity of incorporating deviations from axial symmetry within the model to capture the subtle low-spin spectral variations and shape dynamics observed in this nucleus.

A notable discrepancy is observed in the $2_2^+ \to 3_1^+$ transition, where the experimentally deduced matrix element is approximately half the magnitude of its predicted value. This

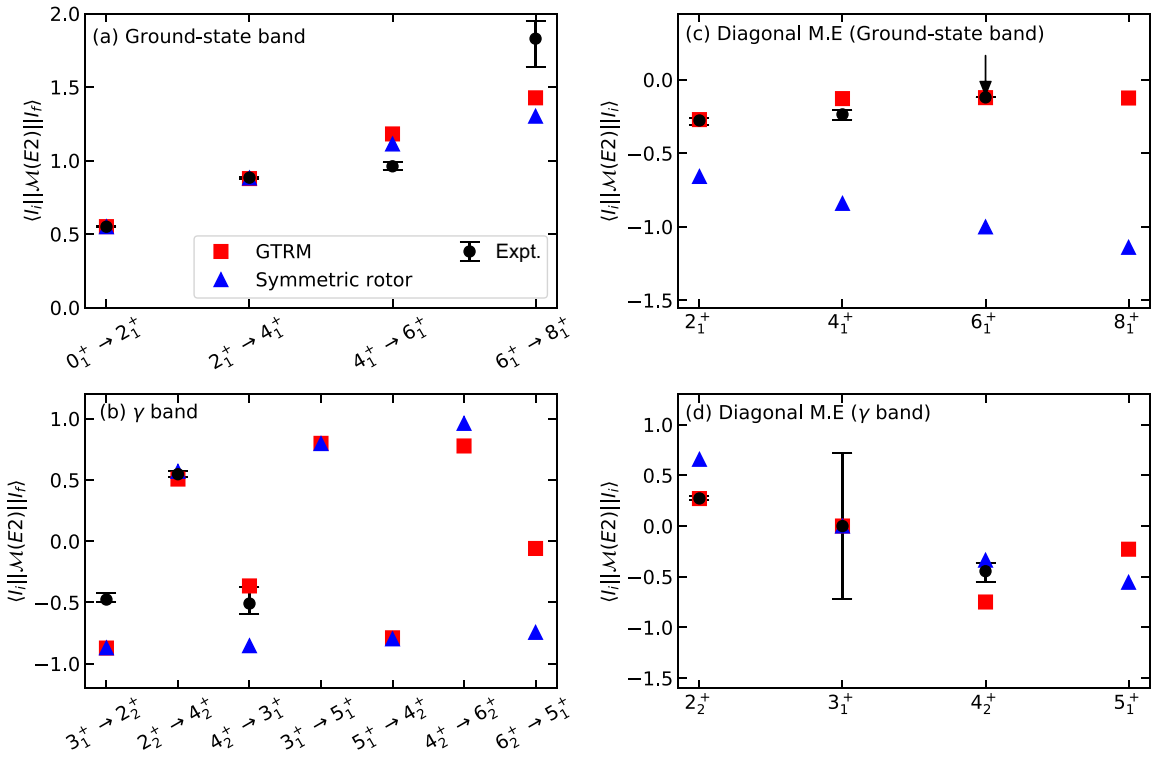

FIG. 6. Experimental transition matrix elements for intraband transitions, $\langle I_i||\mathcal{M}(E2)|I_f\rangle$ for the (a) ground-state and (b) γ bands in comparison with calculations using the generalized triaxial rotor model (GTRM) with the full-diagonalization of the triaxial rotor and the symmetric rotor model. [(c) and (d)] Similar comparisons for diagonal matrix elements $\langle I_i||\mathcal{M}(E2)||I_i\rangle$ for the ground-state and γ bands. The upper limit for the 6_1^+ diagonal matrix element has been denoted by a downward-pointing arrow.

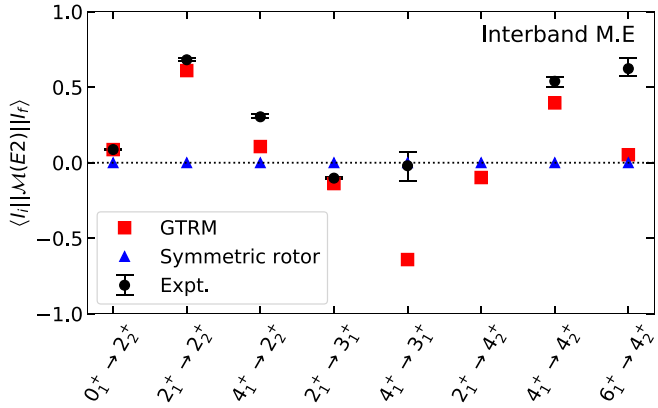

FIG. 7. Experimental transition matrix elements for interband transitions between the ground-state and γ bands in comparison with calculations using the generalized triaxial rotor model (GTRM) with the full-diagonalization of the triaxial rotor and the symmetric rotor model.

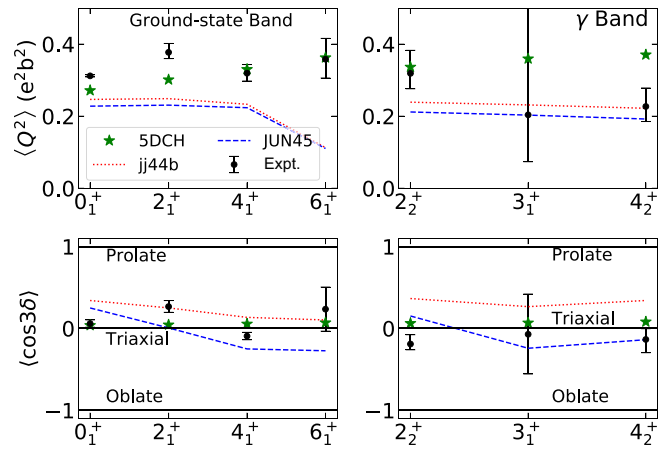

FIG. 8. $\langle Q^2\rangle$ (top) and $\langle\cos 3\delta\rangle$ (bottom) values derived from the invariant sum-rule analysis for the ground-state (left) and the γ bands (right). The green stars are the predictions from the five-dimensional collective Hamiltonian (5DCH) calculations (see text). The blue dashed and the red dotted lines indicate shell-model predictions for the JUN45 and jj44b interactions, respectively. Limits for the various shapes are indicated by the dashed lines.

difference could stem from several potential factors, including inaccuracies in the available spectroscopic data, exclusion of effects related to shape coexistence or γ softness within the model, or that the 3_1^+ state is not directly excited via Coulomb excitation but is instead populated through deexcitation γ rays, which may influence the observed matrix element. The experimental transition matrix elements for interband transitions between the ground-state and γ bands as well as the GTRM and the symmetric rotor model predictions are presented in Fig. 7. Since the symmetric rotor model does not account for mixing between bands, it does not allow transitions between the ground-state and γ bands and, hence, reports a zero value for all the interband transition matrix elements (see Fig. 7). In contrast, the asymmetry in the electric tensor inherent in the GTRM allows for transitions between these bands. The GTRM model, hence, reproduces the experimental data better, as seen in Fig. 7.

C. Quadrupole invariants

The complete set of $E2$ matrix elements extracted from these Coulomb excitation measurements enables the construction of quadrupole invariants ($\langle Q^2\rangle$ and $\langle\cos 3\delta\rangle$). In turn, these provide the opportunity to investigate quantitatively the quadrupole collectivity of the low-lying ^{74}Ge states and the associated shapes, based on the model-independent invariant sum rules of Kumar [33] and Cline [34]. For each specific level, the quadrupole invariant $\langle Q^2\rangle$ represents the expectation value of the sum of products of all $E2$ matrix elements linked to it, while the $\langle\cos 3\delta\rangle$ quantity characterizes its axial asymmetry. These invariants describe the nuclear charge distribution of a charged ellipsoid in terms of the collective deformation parameters; i.e., the overall quadrupole deformation, β, and triaxiality parameter, δ. Assuming a nonrigid deformation, Ref. [35] gives the following expressions for the effective values of the shape invariants:

$$\beta_{\text{eff}} = \frac{4\pi}{3ZR^2}\sqrt{\langle Q^2\rangle} \tag{1}$$

and

$$\delta_{\text{eff}} = \tfrac{1}{3}\arccos(\langle\cos 3\delta\rangle). \tag{2}$$

The experimental quadrupole invariants, $\langle Q^2\rangle$ and $\langle\cos 3\delta\rangle$, for the states within the ground-state and the γ bands, are presented in Fig. 8. An almost constant, nonzero value of $\langle Q^2\rangle$ indicates that ^{74}Ge is deformed in its ground-state band and confirms the presence of strong correlations between the $E2$ properties. Much like the ^{72,76}Ge cases [5,10], both the ground-state and γ bands in ^{74}Ge are characterized by the same $\langle Q^2\rangle$ values within the errors. Over the observed spin range, the average $\langle Q^2\rangle$ value of 0.30 e^2 b^2 corresponds to a quadrupole deformation of $\beta_{\text{eff}} \approx 0.28$ [using Eq. (1)] for both bands.

In addition, the behavior of $\langle\cos 3\delta\rangle$ [Fig. 8 (bottom)] is consistent with a triaxially deformed shape for both bands, and the derived average $\langle\cos 3\delta\rangle$ value of 0.15 corresponds to $\delta_{\text{eff}} \approx 27^\circ$ [using Eq. (2)], which matches expectations for a well-defined triaxial shape. Although a good estimate of the asymmetry angle is obtained from this value of $\langle\cos 3\delta\rangle$, it is not sensitive to dynamic shape fluctuations and, therefore, cannot distinguish between soft and rigid triaxiality. The relative softness in $\langle Q^2\rangle$ and $\langle\cos 3\delta\rangle$ can be quantified by evaluating their respective variances, $\sigma\langle Q^2\rangle$ and $\sigma\langle\cos 3\delta\rangle$, which reflect intrinsic shape fluctuations. These quantities are derived from higher-order quadrupole shape invariants using the SIGMA code [23] and provide a measure of the degree of β and γ softness of the nuclear potential. These variances are found in Fig. 9 for the three-lowest lying 0_1^+, 2_1^+, and 2_2^+ states in ^{74}Ge. The $\sigma\langle\cos 3\delta\rangle$ quantity is a measure of how much the quadrupole asymmetry parameter $\langle\cos 3\delta\rangle$ fluctuates due to nuclear shape dynamics. This quantity helps distinguish between rigid triaxial, γ-soft, and harmonic vibrational nuclei. The various values that $\sigma\langle\cos 3\delta\rangle$ can take and their corresponding descriptions are provided in Table IV.

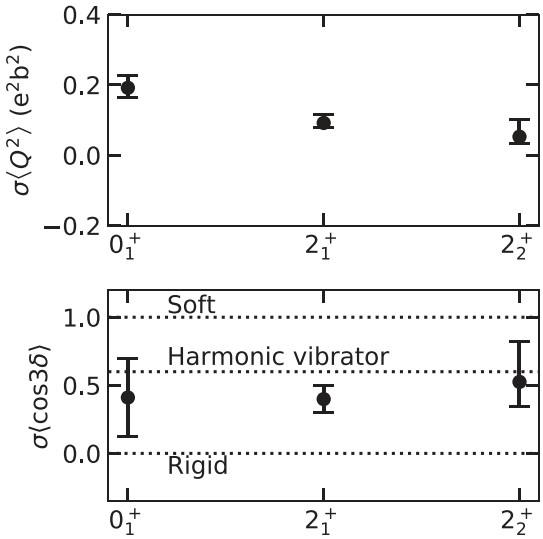

FIG. 9. Statistical dispersion of the (top) quadrupole deformation $\sigma\langle Q^2\rangle$ and (bottom) asymmetry $\sigma\langle\cos 3\delta\rangle$ for the 0_1^+ and $2_{1,2}^+$ states in ^{74}Ge.

In the bottom panel, the spread in the $\langle\cos 3\delta\rangle$ values is consistent with the behavior expected for a harmonic vibrator, a view further reinforced by the nonzero values of $\sigma\langle Q^2\rangle$, depicted in the top panel. This suggests that ^{74}Ge is a transitional nucleus, lying in between the γ-soft ^{72}Ge [5] and the γ-rigid ^{76}Ge [10] neighboring isotopes. However, this interpretation appears somewhat inconsistent with the experimental $\langle Q^2\rangle$ values displayed in Fig. 8. For a harmonic vibrator, $\langle Q^2\rangle$ is expected to increase monotonically with spin; instead, the observed values remain nearly constant within the experimental uncertainties. As noted earlier, a constant quadrupole invariant indicates that the nuclear shape remains relatively unchanged with increasing spin (which can be referred to as β rigidity). However, the nonzero variance in $\langle Q^2\rangle$ [Fig. 9 (top)] reveals that the nucleus is not perfectly rigid—there are small residual fluctuations indicating minor β softness. Thus, the experimental data point to a low-lying structure of ^{74}Ge that lies between the extremes of shape softness and rigidity.

TABLE IV. Description of the various values that $\sigma\langle\cos 3\delta\rangle$ can take. Definitions and descriptions taken from Refs. [33,34,36].

$\sigma\langle\cos 3\delta\rangle$	Nuclear shape model	Description
≈0.0	Rigid triaxial rotor	The nucleus has a well-defined γ, meaning no fluctuations
≈1.0	Soft triaxial rotor	The nucleus fluctuates significantly in γ, but still within a deformed shape
≈0.6	Harmonic quadrupole vibrator	The nucleus undergoes large, symmetric quadrupole shape vibrations around sphericity

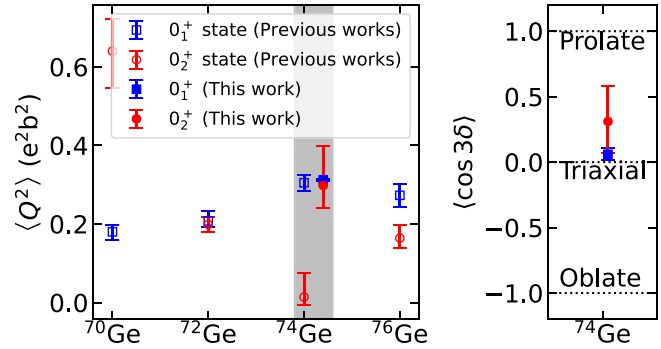

FIG. 10. $\langle Q^2\rangle$ values for the 0_1^+ and the 0_2^+ states in the ^{70,72,74,76}Ge isotopes (left) and $\langle\cos 3\delta\rangle$ invariant for these two states in ^{74}Ge (right). The $\langle Q^2\rangle$ values for ^{70,72}Ge are taken from Refs. [37] and [5], respectively. For ^{74}Ge, the previous $\langle Q^2\rangle$ values are obtained from Ref. [13] while those for ^{76}Ge are from Ref. [38].

Figure 10 displays the experimental quadrupole invariants for the 0_1^+ and 0_2^+ states in ^{74}Ge and compares the values with those from the previous Coulomb excitation measurement by Toh *et al.* [13]. This figure also includes these invariants for the neighboring even Ge isotopes [5,10,37]. For the case of ^{70}Ge, the 0_2^+ level has been reported to be more deformed than the 0_1^+ one [37]. For ^{72}Ge, however, the two 0^+ states were found to have essentially the same $\langle Q^2\rangle$ value [5]. The change between ^{70}Ge and ^{72}Ge seen in Fig. 10 points to a subtle shape transition with the ground-state configuration of ^{70}Ge transitioning into the 0_2^+ excited one in ^{72}Ge, a characteristic extending further to the heavier even Ge isotopes. These 0_2^+ levels in ^{74,76}Ge were predicted to be spherical, with the 0_1^+ ground states being deformed [7]. However, the present analysis indicates that a considerable deformation is associated with the ^{74}Ge, 0_2^+ level. As discussed above, this is partly due to the role of the $0_2^+ \rightarrow 2_3^+$ transition observed here for the first time with the associated matrix element contributing significantly to the sum rule. Such a situation was reported in ^{72}Ge as well with a strong contribution from the $0_2^+ \rightarrow 2_3^+$ matrix element leading to a 0_2^+ state with a deformation comparable to the ground-state one [5]. A similar conclusion can now be drawn for the case of ^{74}Ge, where the 0_2^+ state has been observed to be equally deformed as the 0_1^+ one. The situation evolves further in ^{76}Ge with this 0_2^+ level becoming slightly less deformed than the 0_1^+ ground state. The trend in $\langle Q^2\rangle$ for the ^{70,72,74,76}Ge isotopes is presented in Fig. 10, where a direct evidence of the shape transition occurring within the stable even Ge isotopes is observed with the 0_1^+ and 0_2^+ states exchanging character in transitional ^{72}Ge. The right panel of Fig. 10 provides the $\langle\cos 3\delta\rangle$ invariants for the 0_1^+ and the 0_2^+ levels in ^{74}Ge. Both these 0^+ states have values consistent with a triaxial deformation. In the neighboring ^{72}Ge nucleus, the 0_2^+ state is the first excited state and has been identified as part of a coexisting triaxial configuration [5]. Although the 0_2^+ state in ^{74}Ge appears at slightly higher energy, the similar deformation characteristics of both $0_{1,2}^+$ states suggest a possible analogous case of triaxial shape coexistence.

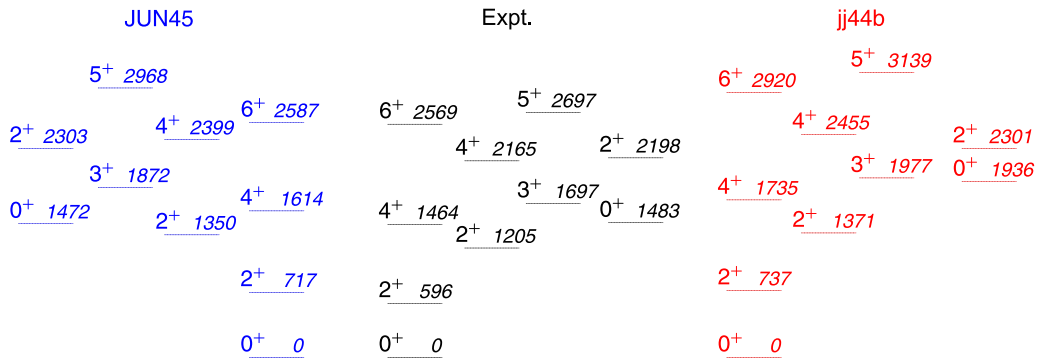

FIG. 11. Experimental level energies in ^{74}Ge compared with the large-scale shell-model calculations using the jj44b and JUN45 effective interactions. The experimental energies are given in black (center), the jj44b predictions are in red (right), and the JUN45 ones are in blue (left).

D. Large-scale shell-model calculations

Large-scale shell-model calculations were carried out within the jj44b model space composed of a ^{56}Ni inert core and the $0f_{7/2}$, $1p_{3/2}$, $1p_{1/2}$, and $0g_{9/2}$ valence proton and neutron orbitals. The calculations were performed using the shell-model code `NuShellX` [39] with both the jj44b and JUN45 Hamiltonians and effective charges of $e_\pi = 1.500$ and $e_\nu = 1.100$. More details about these calculations are available in Refs. [25,40].

The comparison between experimental and computed level energies, presented in Fig. 11, includes levels up to 6^+ in the ground-state band and 5^+ in the γ band, as well as the nonyrast 0_2^+ and 2_3^+ states. The data are better reproduced with the JUN45 interaction, with the jj44b one consistently predicting higher excitation energies for levels in both bands. The nonyrast 0_2^+ and 2_3^+ states are also reasonably reproduced by JUN45. A root-mean-square deviation of $\Delta_{\rm rms} = 151$ keV was obtained when comparing data and predictions with the JUN45 interaction while a much larger $\Delta_{\rm rms} = 286$ keV was obtained with the jj44b one.

The measured spectroscopic quadrupole moments, $Q_s(I)$, are compared with the corresponding shell-model results from both Hamiltonians in Fig. 12. The $Q_s(I)$ values for the 2_1^+ and 2_2^+ states reported in Ref. [13] are also included, as they agree well with the results of the present work. As can be seen in the figure, most $Q_s(I)$ moments are reproduced with suitable accuracy, with the exception of those associated with the 3_1^+ level of the γ band, where, as noted earlier, the large discrepancies may be due to inaccurate spectroscopic information, the omission of shape coexistence and γ softness effects in the model, or the indirect population of this state via deexcitation γ rays rather than direct Coulomb excitation. Figure 12 indicates that, unlike the excitation energies, the experimental $Q_s(I)$ moments are better reproduced by the jj44b interaction. The latter calculations reproduce the prolate deformation for the ground-state band as well as for the γ band very well. In contrast, JUN45 predictions, although matching well in magnitude, are of the opposite sign for all levels of both bands with the exception of the 3_1^+ and 2_3^+ states. These calculated positive quadrupole moments result in an oblate deformation, which contradicts the present experimental results.

The measured matrix elements were also used to deduce reduced transition probabilities, $B(E2)$, for transitions within the ground-state and γ bands. These are presented in Table V along with those associated with the nonyrast 0_2^+, 2_3^+, and 0_3^+ states. The last two columns list the corresponding $B(E2)$ values calculated with the jj44b and JUN45 interactions. Both of these reproduce well the transition strengths within the yrast band ($2_1^+ \to 0_1^+$, $4_1^+ \to 2_1^+$, and $6_1^+ \to 4_1^+$), with the JUN45 interaction performing better for all three transitions. The small $B(E2)$ experimental value of ∼0.8 W.u. for the $2_2^+ \to 0_1^+$ transition, and the much larger value of ∼50 W.u. for the $2_2^+ \to 2_1^+$ one, are also accounted for reasonably well by both interactions. However, as seen in Table V, the JUN45 interaction offers a more accurate representation of the former strength, whereas the jj44b interaction tends to slightly underestimate it. In contrast, for the latter strength, both interactions demonstrate comparable performance, with jj44b overestimating and JUN45 underestimating by approximately six units. Overall, the JUN45 Hamiltonian was found to reproduce the experimental $B(E2)$ values better than the

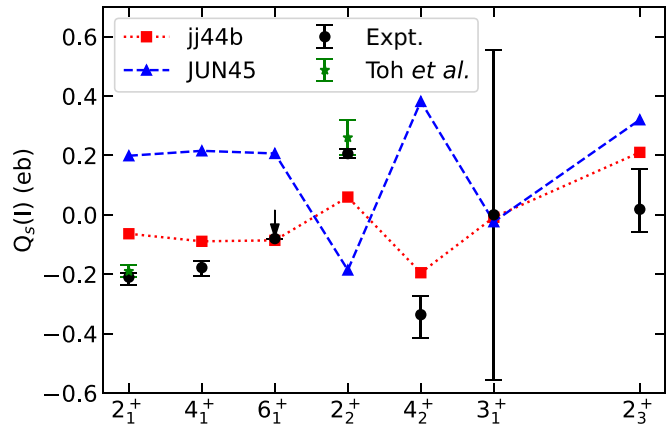

FIG. 12. Large-scale shell model predictions and previously reported [13] quadrupole moments, $Q_s(I)$, in comparison with the experimental values deduced from the measured diagonal matrix elements. The upper limit for the quadrupole moment of 6_1^+ state is marked with a downward-pointing arrow.

TABLE V. Comparison of experimental reduced transition probabilities with those obtained from shell-model calculations using the jj44b and JUN45 effective interactions.

	$B(E2; I_i \to I_f)$ W.u.		
$I_i \to I_f$	Exp	jj44b	JUN45
$2_1^+ \to 0_1^+$	32.8(3)	38.4	32.2
$2_2^+ \to 0_1^+$	0.83(3)	0.09	1.3
$2_2^+ \to 2_1^+$	$50.3^{+1.3}_{-0.8}$	55.9	43.6
$4_1^+ \to 2_1^+$	47.0(7)	53.2	46.7
$4_1^+ \to 2_2^+$	10(1)	0.0003	0.004
$0_2^+ \to 2_1^+$	28(1)	2.03	15.5
$0_2^+ \to 2_2^+$	18(4)	19.8	0.9
$3_1^+ \to 2_1^+$	$0.81^{+0.18}_{-0.05}$	0.2	1.9
$3_1^+ \to 2_2^+$	18^{+4}_{-1}	61	52.3
$2_3^+ \to 0_1^+$	0.18(3)	0.004	0.09
$2_3^+ \to 2_1^+$	$0.08^{+0.09}_{-0.08}$	0.09	0.2
$2_3^+ \to 2_2^+$	1.9(7)	1.2	0.1
$2_3^+ \to 0_2^+$	18^{+3}_{-1}	30	10.2
$4_2^+ \to 2_2^+$	18^{+2}_{-1}	21.5	11.7
$4_2^+ \to 4_1^+$	18(2)	19.4	17.5
$4_2^+ \to 3_1^+$	20^{+12}_{-6}	1.5	13.4
$6_1^+ \to 4_1^+$	39(2)	59.3	49
$6_1^+ \to 4_2^+$	23^{+6}_{-4}	0.002	0.3
$0_3^+ \to 2_1^+$	1.4(7)	5.2	0.1
$0_3^+ \to 2_2^+$	5^{+12}_{-5}	3.2	14

jj44b one, with a few exceptions such as the $4_1^+ \to 2_2^+$ transition, where the strength is vastly underestimated. These observations align with those reported in Ref. [11] which also favored JUN45 for the experimental excitation energies but jj44b for the spectroscopic quadrupole moments. In the case of ^{74}Ge, the JUN45 interaction was also favored somewhat for the description of the strengths of M1 transitions from 1^- states, in the 2–5 MeV excitation-energy range as populated in nuclear resonance fluorescence [40].

E. Covariant density functional theory and five-dimensional collective Hamiltonian calculations

To gain further insight into the characteristics of the observed low-lying bands, calculations utilizing constrained covariant density functional theory (CDFT) [41–44] were carried out. The first step of this study was aimed at determining the topology of the potential energy surface (PES) for the ground-state configuration, as obtained through CDFT calculations with the PC-PK1 effective interaction [45]. In solving the Dirac equation for nucleons, a three-dimensional harmonic oscillator basis spanning 12 major oscillator shells was employed. Furthermore, a density-independent δ force was incorporated in the particle-particle channel, with strength parameters of 349.5 and 330.0 MeV fm^3 for neutrons and protons, respectively. To construct the PES, the (β, γ) deformation parameters were varied within specified intervals of $0.0 \leqslant \beta \leqslant 0.6$ and $0^\circ \leqslant \gamma \leqslant 60^\circ$, in step sizes of $\Delta\beta = 0.05$ and $\Delta\gamma = 6^\circ$, respectively. The resulting PES in the β-γ plane is presented in Fig. 13, with energy values normalized to the binding energy of the absolute minimum which is marked by a pink star. Similar potential energy surfaces have been provided in previous studies [46,47]. The analysis reveals that the ^{74}Ge ground state exhibits a deformation characterized by $(\beta, \gamma) = (0.25, 30^\circ)$, with a notable softness in the γ direction.

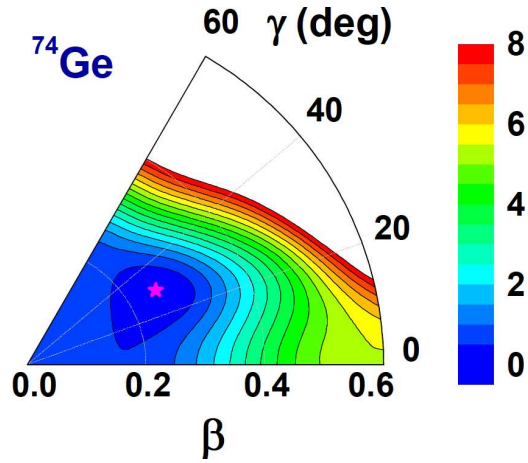

FIG. 13. Potential energy surface in the β-γ plane ($0 \leqslant \beta \leqslant 0.6$, $0^\circ \leqslant \gamma \leqslant 60^\circ$) for the ground-state configuration of ^{74}Ge from CDFT calculations with the PC-PK1 effective interaction. Energies depicted on the plot are normalized relative to the absolute minimum energy (in MeV), denoted by a pink star symbol. Contour lines on the graph are separated by 0.5 MeV.

With the collective potential, moments of inertia, and mass parameters determined from the CDFT, a five-dimensional collective Hamiltonian (5DCH) [48–52] was then constructed. This approach restores rotational symmetry and accounts for triaxial shape fluctuations. Diagonalizing the 5DCH yields the collective energies and wave functions at each given spin. From the 5DCH wave functions, the expectation values of the overall deformation, $\langle Q^2 \rangle$, and the asymmetry, $\langle \cos 3\delta \rangle$, were calculated using the method described in Ref. [53] and the expressions:

$$Q^2 = q_0^2(\beta^2 + 2C\beta^3 \cos 3\gamma + C^2\beta^4), \tag{3}$$

$$\cos 3\delta = q_0^3(\beta^3 \cos 3\gamma + 3C\beta^4 + 3C^2\beta^5 \cos 3\gamma + 2C^3\beta^6 \cos^2 3\gamma - C^3\beta^6), \tag{4}$$

with

$$q_0 = \frac{3}{4\pi} ZR^2, \tag{5}$$

$$R = R_0(1 - 12C^2\beta^2 + 16C^3\beta^3 \cos 3\gamma)^{-1/3}, \tag{6}$$

$$R_0 = 1.2A^{1/3}\,\text{fm}, \quad C = \sqrt{\frac{5}{64\pi}}. \tag{7}$$

The resulting $\langle Q^2 \rangle$ and $\langle \cos 3\delta \rangle$ rotational invariants derived from the 5DCH calculations for the ground-state and γ bands are displayed in Fig. 8, alongside the present experimental data. The agreement between these calculations and the experimental data is notable, further reinforcing the

TABLE VI. Comparison of rotational invariants deduced from the experiment with those obtained from the five-dimensional collective Hamiltonian (5DCH) calculations for the 0_1^+ and 0_2^+ states. For completeness, the fluctuations in the invariants obtained for the 0_1^+ state are also provided.

	0_1^+		0_2^+	
	exp	5DCH	exp	5DCH
$\langle Q^2 \rangle$	0.312(3)	0.271	$0.30^{+0.10}_{-0.05}$	0.289
$\sigma\langle Q^2 \rangle$	0.19(3)			
$\langle \cos 3\delta \rangle$	0.06(4)	0.037	$0.3^{+0.3}_{-0.2}$	0.073
$\sigma\langle \cos 3\delta \rangle$	0.4(3)			

significance of triaxiality in accurately describing the low-lying structure of ^{74}Ge. Furthermore, the 5DCH model predictions of the $\langle Q^2 \rangle$ and $\langle \cos 3\delta \rangle$ invariants for the 0_1^+ and 0_2^+ states are compared with the experimental values in Table VI. The close similarity between the theoretical predictions and experimental observations is again notable. Specifically, it provides further compelling evidence for the triaxial nature of the 0_2^+ level.

V. CONCLUSIONS

A detailed analysis of the deformation properties of the low-lying states of ^{74}Ge has been carried out following a multistep Coulomb excitation measurement performed with the GRETINA γ-ray tracking array and the CHICO2 particle detector. A complete set of reduced $E2$ transition and diagonal matrix elements was obtained using the semiclassical coupled-channels code GOSIA. The data were compared with results of theoretical calculations carried out within the framework of the generalized triaxial rotor model. These reproduced the experimental matrix elements accurately and provided further support for the triaxial interpretation of the underlying ^{74}Ge structure. Further interpretation within the framework of the shell model as well as within the covariant density functional theory combined with the five-dimensional collective Hamiltonian also achieved a satisfactory reproduction of the experimental observations. The present analysis supports a triaxial character for both the $0_{1,2}^+$ states in ^{74}Ge. These findings point to a structural similarity with the neighboring nucleus ^{72}Ge, where triaxial shape coexistence between the 0_1^+ and 0_2^+ states has been firmly established. This suggests the possibility of a comparable coexistence scenario in ^{74}Ge and further stresses the importance of measurements like those presented here for developing a comprehensive understanding of even-even nuclei in this mass region.

ACKNOWLEDGMENTS

This work was supported in part by the U.S. DOE, Office of Science, Office of Nuclear Physics, under Grants No. DE-SC0023010 (UNC), No. DE-FG02-97ER41041 (UNC), No. DE-FG02-97ER41033 (TUNL), No. DE-AC02-06CH11357, No. DE-AC05-00OR22725 (ORNL) and Grants No. DE-FG02-94ER40834, No. DE-FG02-08ER41556, No. DE-FG02-94ER40848, and No. DE-SC0020451; by the NSF under Contracts No. PHY-0606007, No. PHY-2011890, No. PHY-2208137, and No. PHY-2310059; by the UNC Startup Funds of ADA; by the National Natural Science Foundation of China under Grant No. 12205103; and by the National Key R&D Program of China Grants No. 2024YFE0109800 and No. 2024YFE0109803. Work at Lawrence Livermore National Laboratory was performed under the auspices of the U.S. Department of Energy under Contract No. DE-AC52-07NA27344. Work at Los Alamos National Laboratory, operated by Triad National Security, LLC, for the National Nuclear Security Administration of the U.S. Department of Energy was done under Contract No. 89233218CNA000001. GRETINA was funded by the U.S. DOE, Office of Science, Office of Nuclear Physics, and operated by the ANL and LBNL, under Contract No. DEAC02-05CH11231 (LBNL). This research used the resources of Argonne National Laboratory's ATLAS facility, a DOE Office of Science User Facility.

DATA AVAILABILITY

The data that support the findings of this article are not publicly available because they are owned by a third party and the terms of use prevent public distribution. The data are available from the authors upon reasonable request.

[1] W. Nazarewicz, J. Dudek, R. Bengtsson, T. Bengtsson, and I. Ragnarsson, Nucl. Phys. A **435**, 397 (1985).
[2] P. Sarriguren, E. Moya de Guerra, and A. Escuderos, Nucl. Phys. A **658**, 13 (1999).
[3] M. Yamagami, K. Matsuyanagi, and M. Matsuo, Nucl. Phys. A **693**, 579 (2001).
[4] M. Bender, P. Bonche, and P.-H. Heenen, Phys. Rev. C **74**, 024312 (2006).
[5] A. Ayangeakaa, R. Janssens, C. Wu, J. Allmond, J. Wood, S. Zhu, M. Albers, S. Almaraz-Calderon, B. Bucher, M. Carpenter, C. Chiara, D. Cline, H. Crawford, H. David, J. Harker, A. Hayes, C. Hoffman, B. Kay, K. Kolos, A. Korichi *et al.*, Phys. Lett. B **754**, 254 (2016).
[6] S. Iwasaki, T. Marumori, F. Sakata, and K. Takada, Prog. Theor. Phys. **56**, 1140 (1976).
[7] K. Heyde and J. L. Wood, Rev. Mod. Phys. **83**, 1655(E) (2011).
[8] L. Guo, J. A. Maruhn, and P.-G. Reinhard, Phys. Rev. C **76**, 034317 (2007).
[9] Y. Toh, C. J. Chiara, E. A. McCutchan, W. B. Walters, R. V. F. Janssens, M. P. Carpenter, S. Zhu, R. Broda, B. Fornal, B. P. Kay, F. G. Kondev, W. Królas, T. Lauritsen, C. J. Lister, T. Pawłat, D. Seweryniak, I. Stefanescu, N. J. Stone, J. Wrzesiński, K. Higashiyama *et al.*, Phys. Rev. C **87**, 041304(R) (2013).
[10] A. D. Ayangeakaa, R. V. F. Janssens, S. Zhu, D. Little, J. Henderson, C. Y. Wu, D. J. Hartley, M. Albers, K. Auranen, B. Bucher, M. P. Carpenter, P. Chowdhury, D. Cline, H. L.

Crawford, P. Fallon, A. M. Forney, A. Gade, A. B. Hayes, F. G. Kondev, Krishichayan *et al.*, Phys. Rev. Lett. **123**, 102501 (2019).
[11] A. D. Ayangeakaa, R. V. F. Janssens, S. Zhu, J. M. Allmond, B. A. Brown, C. Y. Wu, M. Albers, K. Auranen, B. Bucher, M. P. Carpenter, P. Chowdhury, D. Cline, H. L. Crawford, P. Fallon, A. M. Forney, A. Gade, D. J. Hartley, A. B. Hayes, J. Henderson, F. G. Kondev *et al.*, Phys. Rev. C **107**, 044314 (2023).
[12] G. H. Bhat, W. A. Dar, J. A. Sheikh, and Y. Sun, Phys. Rev. C **89**, 014328 (2014).
[13] Y. Toh, T. Czosnyka, M. Oshima, T. Hayakawa, H. Kusakari, M. Sugawara, Y. Hatsukawa, J. Katakura, N. Shinohara, and M. Matsuda, Eur. Phys. J. A **9**, 353 (2000).
[14] S. Paschalis, I. Lee, A. Macchiavelli, C. Campbell, M. Cromaz, S. Gros, J. Pavan, J. Qian, R. Clark, H. Crawford, D. Doering, P. Fallon, C. Lionberger, T. Loew, M. Petri, T. Stezelberger, S. Zimmermann, D. Radford, K. Lagergren, D. Weisshaar *et al.*, Nucl. Instrum. Methods A **709**, 44 (2013).
[15] C. Wu, D. Cline, A. Hayes, R. Flight, A. Melchionna, C. Zhou, I. Lee, D. Swan, R. Fox, and J. Anderson, Nucl. Instrum. Methods A **814**, 6 (2016).
[16] B. Schürmann, D. Rychel, B. van Krüchten, J. Speer, and C. Wiedner, Nucl. Phys. A **475**, 361 (1987).
[17] R. Tamisier, B. Ramstein, P. Avignon, L. Rosier, G. La Rana, F. Guilbault, C. Lebrun, and C. Jeanperrin, Nucl. Phys. A **385**, 430 (1982).
[18] K. C. Chung, A. Mittler, J. D. Brandenberger, and M. T. McEllistrem, Phys. Rev. C **2**, 139 (1970).
[19] D. C. Camp, D. R. Fielder, and B. P. Foster, Nucl. Phys. A **163**, 145 (1971).
[20] D. Ardouin, D. L. Hanson, and N. Stein, Phys. Rev. C **22**, 2253 (1980).
[21] S. Lafrance, S. Mordechai, H. Fortune, and R. Middleton, Nucl. Phys. A **307**, 52 (1978).
[22] R. E. Chrien, D. I. Garber, J. L. Holm, and K. Rimawi, Phys. Rev. C **9**, 1839 (1974).
[23] T. Czosnyka, D. Cline, A. B. Hayes, P. Napiorkowski, N. Warr, and C. Y. Wu, Bull. Amer. Phys. Soc. **28**, 745 (1983).
[24] B. Singh and A. R. Farhan, Nucl. Data Sheets **107**, 1923 (2006).
[25] E. E. Peters, B. A. Brown, S. Mukhopadhyay, A. P. D. Ramirez, and S. W. Yates, Phys. Rev. C **109**, 054318 (2024).
[26] R. Lecomte, M. Irshad, S. Landsberger, G. Kajrys, P. Paradis, and S. Monaro, Phys. Rev. C **22**, 2420 (1980).
[27] J. L. Wood, A.-M. Oros-Peusquens, R. Zaballa, J. M. Allmond, and W. D. Kulp, Phys. Rev. C **70**, 024308 (2004).
[28] W. D. Kulp, J. M. Allmond, P. Hatcher, J. L. Wood, J. Loats, P. Schmelzenbach, C. J. Stapels, K. S. Krane, R.-M. Larimer, and E. B. Norman, Phys. Rev. C **73**, 014308 (2006).
[29] J. M. Allmond, R. Zaballa, A. M. Oros-Peusquens, W. D. Kulp, and J. L. Wood, Phys. Rev. C **78**, 014302 (2008).
[30] J. M. Allmond, J. L. Wood, and W. D. Kulp, Phys. Rev. C **80**, 021303(R) (2009).
[31] J. M. Allmond, J. L. Wood, and W. D. Kulp, Phys. Rev. C **81**, 051305(R) (2010).
[32] J. M. Allmond, Ph.D. thesis, Georgia Institute of Technology, 2007.
[33] K. Kumar, Phys. Rev. Lett. **28**, 249 (1972).
[34] D. Cline, Annu. Rev. Nucl. Part. Sci. **36**, 683 (1986).
[35] V. Werner, N. Pietralla, P. von Brentano, R. F. Casten, and R. V. Jolos, Phys. Rev. C **61**, 021301(R) (2000).
[36] C. Wu, D. Cline, T. Czosnyka, A. Backlin, C. Baktash, R. Diamond, G. Dracoulis, L. Hasselgren, H. Kluge, B. Kotlinski, J. Leigh, J. Newton, W. Phillips, S. Sie, J. Srebrny, and F. Stephens, Nucl. Phys. A **607**, 178 (1996).
[37] M. Sugawara, Y. Toh, T. Czosnyka, M. Oshima, T. Hayakawa, H. Kusakari, Y. Hatsukawa, J. Katakura, N. Shinohara, M. Matsuda, T. Morikawa, A. Seki, and F. Sakata, Eur. Phys. J. A **16**, 409 (2003).
[38] A. D. Ayangeakaa (private communication).
[39] B. Brown and W. Rae, Nucl. Data Sheets **120**, 115 (2014).
[40] S. R. Johnson, R. V. F. Janssens, U. Friman-Gayer, B. A. Brown, B. P. Crider, S. W. Finch, Krishichayan, D. R. Little, S. Mukhopadhyay, E. E. Peters, A. P. D. Ramirez, J. A. Silano, A. P. Tonchev, W. Tornow, and S. W. Yates, Phys. Rev. C **108**, 024315 (2023).
[41] J. Meng, J. Peng, S. Q. Zhang, and S.-G. Zhou, Phys. Rev. C **73**, 037303 (2006).
[42] J. Meng, H. Toki, S. Zhou, S. Zhang, W. Long, and L. Geng, Prog. Part. Nucl. Phys. **57**, 470 (2006).
[43] J. Meng, J. Y. Guo, Z. P. Li, H. Z. Liang, W. H. Long, Y. F. Niu, Z. M. Niu, J. M. Yao, Y. Zhang, P. W. Zhao, and S. G. Zhou, Prog. Phys. **31**, 199 (2011).
[44] J. Meng, *Relativistic Density Functional for Nuclear Structure* (World Scientific, Singapore, 2016).
[45] P. W. Zhao, Z. P. Li, J. M. Yao, and J. Meng, Phys. Rev. C **82**, 054319 (2010).
[46] J. J. Sun, Z. Shi, X. Q. Li, H. Hua, C. Xu, Q. B. Chen, S. Q. Zhang, C. Y. Song, J. Meng, X. G. Wu, S. P. Hu, H. Q. Zhang, W. Y. Liang, F. R. Xu, Z. H. Li, G. S. Li, C. Y. He, Y. Zheng, Y. L. Ye, D. X. Jiang *et al.*, Phys. Lett. B **734**, 308 (2014).
[47] T. Nikšić, P. Marević, and D. Vretenar, Phys. Rev. C **89**, 044325 (2014).
[48] T. Nikšić, Z. P. Li, D. Vretenar, L. Próchniak, J. Meng, and P. Ring, Phys. Rev. C **79**, 034303 (2009).
[49] Z. P. Li, T. Nikšić, D. Vretenar, J. Meng, G. A. Lalazissis, and P. Ring, Phys. Rev. C **79**, 054301 (2009).
[50] T. Nikšić, D. Vretenar, and P. Ring, Prog. Part. Nucl. Phys. **66**, 519 (2011).
[51] Z. P. Li, T. Nikšić, and D. Vretenar, J. Phys. G: Nucl. Part. Phys. **43**, 024005 (2016).
[52] Z. P. Li and D. Vretenar, *Model for Collective Motion* (Springer Nature Singapore, Singapore, 2023), pp. 1977–2009.
[53] J. Srebrny, T. Czosnyka, C. Droste, S. Rohoziński, L. Próchiak, K. Zajäc, K. Pomorski, D. Cline, C. Wu, A. Bäcklin, L. Hasselgren, R. Diamond, D. Habs, H. Kömer, F. Stephens, C. Baktash, and R. Kostechi, Nucl. Phys. A **766**, 25 (2006).